Algorithm Theoretical Basis Document

Fusion of VIIRS and CrIS data to construct infrared (IR) absorption band radiances for VIIRS

Bryan A. Baum[1], W. P. Menzel[2], and E. Weisz[2]

[1]Science and Technology Corp., Madison, WI
[2]SSEC, University of Wisconsin-Madison, Madison, WI

Version 1.1

September 2019

Corresponding author: Dr. Bryan A. Baum, Science and Technology Corporation (STC), Madison, WI 53705. Phone: 608-215-7067; E-mail: baum@stcnet.com

Table of Contents

Table of Contents ii

Abstract 1

1. Introduction 2

2. Data and Methodology 5
2.1 Aqua Platform: MODIS and AIRS 5
2.2 Suomi-NPP platform: VIIRS and CrIS 5
2.3 Methodology for construction of IR band radiances from imager-sounder pair 5
2.4 Post-processing: appending IR band radiances into VIIRS Level-1B granule 8
2.5 Example of fusion process with a MODIS granule 9
2.6 Assessment of radiance uncertainty 10
2.7 Data fusion application to VIIRS and CrIS radiances 11

3. Global results from data fusion 14
3.1 MODIS radiance tests – limitation of sensor zenith angle 14

4. Software and data management 19

6. References 20

Abstract

This document describes methodology to construct MODIS-like infrared (IR) spectral band radiances for VIIRS from merged CrIS and VIIRS data. MODIS has three bands sensitive to CO_2 around 4.3 µm and another four around 15 µm, 2 bands sensitive to H_2O near 6.7 µm, and a band sensitive to ozone near 9 µm. The VIIRS sensor does not have any IR absorption bands, which results in a degradation of the accuracy of the cloud products (cloud mask, cloud top pressure/height and thermodynamic phase) and the moisture products (total precipitable water vapor, upper tropospheric humidity). Further, the lack of IR absorption bands limits applications of Suomi NPP data. We developed an innovative solution to this problem by using VIIRS and CrIS data to construct high spatial resolution spectral bands for VIIRS in the CO_2 (MODIS bands 24, 25 and 33-36), the O_3 (MODIS band 30), and the H_2O (MODIS bands 27 and 28) spectrally sensitive regions. The approach involves first finding a relationship between the high spatial resolution VIIRS IR window bands and the lower spatial resolution CrIS fields of view (FOVs). The relationship is determined for each imager granule using a *k-d* tree (i.e., multidimensional) search that associates each imager pixel with *N* nearby sounder FOVs where the radiances match closely; for our application *N* is chosen to be 5. The hyperspectral sounder radiances are convolved using the desired spectral response function and the *N* resulting radiances are averaged to construct the chosen spectral band radiance for each imager pixel. Our software for deriving the fusion-based spectral bands is mature and has been transitioned into Atmosphere SIPS operations. A benefit of our approach is that we can also construct new spectral band radiances for VIIRS that exclude strong trace gas absorption lines or fulfill other criteria, e.g., water vapor bands with narrower bandwidths. That is, we can construct radiances assuming either continuous or discrete spectral response functions. A further bonus from fusion is the mitigation of detector-to-detector radiometric differences that cause striping and product retrieval uncertainties.

1. Introduction

A primary goal of the NASA Suomi-NPP program is to provide continuity in the Earth science products with those obtained from the Earth Observing System (EOS) Aqua and Terra platforms. The ability to achieve continuity is more straightforward when the information content of the satellite sensors does not change radically, i.e., the radiance measurements are continuous in wavelength. For example, when improvements are made in geostationary imagers, more channels are added to the already existing and historical set of measurements. If measurements are taken for at least the historical set of channels, then the task of building continuous products is straightforward.

The path for polar-orbiting imagers is not as straightforward. The Advanced Very High Resolution Radiometer (AVHRR) has been the imager for the NOAA polar-orbiting platforms since 1978. There have been modifications to the AVHRR over time, e.g., with the addition of a 12-µm channel beginning with the AVHRR-2 series and the addition of a 1.6-µm channel beginning with the AVHRR-3 series.

The MODerate resolution Imaging Spectroradiometer (MODIS) sensors on the Terra and Aqua platforms provide measurements in the infrared (IR) water vapor (at 6.7 µm) and carbon dioxide (4.3- and 15-µm) sensitive bands, as shown in Fig. 1a. These so-called sounding bands are useful because they provide a sense of the vertical structure in an atmospheric column. This is especially important when inferring properties for optically thin clouds such as cirrus (Menzel et al. 2008; Baum et al. 2012). With a better sense of the vertical distribution of the clouds, the inferred cloud properties are more consistent daytime to nighttime, over mountain ranges, and in high latitude regions. Heidinger et al. (2010) employed an optimal estimation (OE) approach using IR bands to infer cloud-top pressure. This study clearly showed how using just a single sounding band at 13.3-µm to supplement the IR window bands improved the analysis of optically thin ice clouds over using only IR window bands. Furthermore, the ability to discriminate between low-level and high-level clouds has been found to be critical for improving the determination of the cloud thermodynamic phase (Baum et al. 2012). The MODIS Collection 6 IR cloud phase software incorporated cloud emissivity ratios to improve high/low cloud discrimination, resulting in a much improved product.

The current polar-orbiting imager is the Visible Infrared Imaging Radiometer Suite (VIIRS). VIIRS has several major improvements to the earlier imagers, including pixel spatial resolution that remains essentially constant across the scan. One of the primary limitations for determining cloud properties with VIIRS is that it has only IR window bands, as shown in Fig. 1b. The information content provided by the VIIRS radiance measurements lies between the AVHRR and MODIS sensors. Without even a single IR carbon dioxide or water-vapor sensitive band, the MODIS-like cloud top pressure/height and phase algorithms cannot be transitioned to VIIRS because of a fundamental loss of information. The lack of any sounding channels primarily impacts the inference of cloud properties including cloud-top height/pressure/temperature and IR thermodynamic phase.

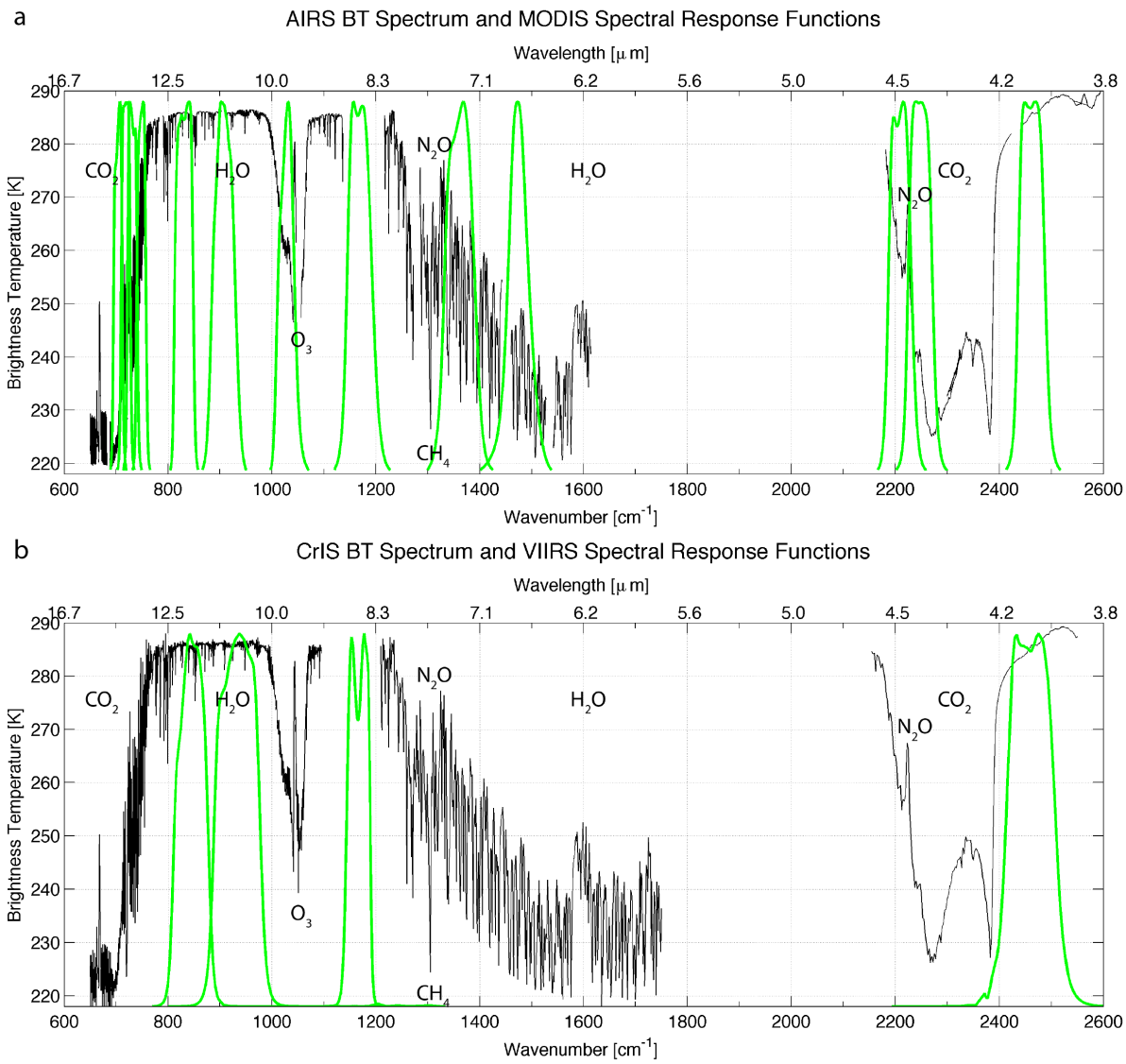

Figure 1: (a) AIRS infrared brightness temperature spectrum (black) with main absorbers indicated, with the MODIS spectral response functions (SRFs; green) superimposed. (b) CrIS infrared brightness temperature spectrum with the VIIRS SRFs superimposed. The spectral response functions are scaled to fit the brightness temperature range.

A comparison of the MODIS and VIIRS IR bands is provided in Table 1.

Table 1: MODIS and VIIRS infrared (IR) bands.

MODIS Infrared bands		VIIRS Infrared bands		Primary Use
band	Central Wavelength [µm]	band	Central Wavelength [µm]	
23	4.05	M13	4.05	Atmospheric temperature
24	4.47			Atmospheric temperature
25	4.52			Atmospheric temperature
27	6.72			Water vapor
28	7.33			Water vapor
29	8.55	M14	8.55	Surface and cloud properties
30	9.73			Ozone
31	11.03	M15	10.76	Surface and cloud properties
32	12.02	M16	12.01	Surface and cloud properties
33	13.34			Cloud properties
34	13.64			Cloud properties
35	13.94			Cloud properties
36	14.23			Cloud properties

An intriguing approach to mitigate this issue was suggested by Cross et al. (2012), who constructed a high spatial resolution (1 km) 13.3-µm CO_2 channel for MODIS by combining the MODIS 11- and 12-µm window channel data with lower spatial resolution 13.3-µm data derived from AIRS. Since MODIS measured radiances at 13.3 µm (band 33), it serves as an ideal platform to test and analyze their method. The constructed radiances were within 1% of the measured radiances within the area where MODIS and AIRS both collect measurements. Outside of the AIRS swath, the results degraded a bit, with a cold bias. The reason for the cold bias is that at high viewing angles, one has to account for the increased absorption due to the path length. This is a systematic bias that can be accounted for using a clear-sky radiative transfer model. The Cross et al. (2013) article provided results for a MODIS granule (5 min) and demonstrated a positive impact on cloud-top height retrievals using the Heidinger OE method.

We expanded upon the Cross et al. (2012) study, comparing MODIS-measured and fusion-constructed 13.3-µm CO_2 bands, and thoroughly tested the fusion-based method using global MODIS measurements. However, during the course of this effort, we found that we can also construct all the other Aqua MODIS IR absorbing bands, with radiances generally within 1% of the original measurements. The results of this work are discussed in Weisz et al. (2017). In this ATBD, we describe the methodology in Weisz et al. (2017) in more detail and provide examples of radiance band construction using both MODIS+AIRS and VIIRS+CrIS.

2. Data and Methodology

2.1 Aqua Platform: MODIS and AIRS

The MODIS sensor is a 36-band whiskbroom scanning radiometer that is currently flying on the NASA Terra and Aqua platforms (Salomonson et al. 1989). The Terra platform, launched in December 1999, is in a daytime descending orbit with an equatorial crossing of 1030 local solar time (LST). The Aqua platform, launched in May 2002, is in a daytime ascending orbit at 1330 LST. The equatorial crossing times have been held constant over the years for both platforms. For our proposed work, we will use the VIIRS Level-1B files for granules of 6 min duration that incorporate the most up-to-date calibration. Because the calibration is expected to change over time, it is likely the Atmosphere SIPS will generate VIIRS Level-1B files on demand that are tailored to the user, who can select which IR bands are required for their application.

The AIRS (Aumann et al. 2003) on the Aqua satellite is a high-spectral-resolution (wavenumber to resolution ratio of 1200) grating spectrometer with 2378 bands in the wavelength regions of 3.7 to 4.61 µm, 6.2 to 8.22 µm, and 8.8 to 15.4 µm. AIRS radiances enable derivation of vertical profiles of atmospheric temperature and water vapor from the earth's surface to TOA with a horizontal resolution of 13.5 km at nadir.

2.2 Suomi-NPP platform: VIIRS and CrIS

The VIIRS sensor is a 22-band scanning radiometer that is currently flying on the NASA Suomi NPP platform. The Suomi NPP platform, launched on 28 October, 2011, is at an altitude of 824 km and has an equatorial crossing of 1330 UTC. VIIRS has 16 bands scanning a 3000 km swath at 750-m resolution (medium resolution, or M), 5 bands at 375 m resolution (imaging, or I), and a day/night band. For this investigation, the focus will be on using the bands at M resolution, for which Level-1B radiances are provided in NetCDF4 for granules of 6 min duration.

The Cross-track Infrared Sounder (CrIS), a Fourier transform spectrometer, has 1305 spectral bands over 3 wavelength ranges: LWIR (9.14 to 15.38 µm); MWIR (5.71 to 8.26 µm); and SWIR (3.92 to 4.64 µm). CrIS scans a 2200 km swath width (± 50 degrees), with 30 Earth-scene views. Each view consists of 9 FOVs from a 3x3 array that have a nadir spatial resolution of approximately 14 km. For the purposes of this proposal, we intend to use the Level 1b granules in NetCDF4, for granules of 6 min duration.

2.3 Methodology for construction of IR band radiances from imager-sounder pair

The construction of high spatial resolution IR band radiances (see Weisz et al. 2017 for more details) consists of two steps: (1) performing a search for N sounder FOVs (here $N = 5$) for each imager pixel using the *k-d* tree search algorithm on both high spatial resolution and low spatial resolution split-window imager radiances, and (2) calculating the convolved sounder radiances for each of the 5 sounder FOVs selected for each imager pixel. To reduce confusion between the imager and sounder spatial resolutions, we use "pixel" for the imager and field of view (FOV) for the sounder. The resulting 5 convolved radiance values are averaged and the average value is reported for each pixel. These two steps are illustrated in Figs. 2 and 3, with discussion below.

Figure 2 shows the methodology of the first step for developing the *k-d* tree search for merged imager and sounder data. The result of the *k-d* tree search determines a set of *N* sounder FOVs for each imager pixel. The specific steps to reach that point are as follows:

1. The Level-2 (L2) imager and sounder radiance and geolocation data are read in. The L2 data are available at the Atmosphere SIPS: http://sips.ssec.wisc.edu.
2. The Atmosphere SIPS provides pre-computed collocation files for the imager/sounder pair; these collocation routines are provided by Greg Quinn and Fred Nagle. Conversely, software exists to perform collocation but this is unnecessary as the SIPS provides the pertinent information.
3. The average of the radiances for all imager pixels within each sounder FOV is computed. This provides low spatial resolution radiance data for each FOV.
4. A nearest neighbor search using the *k-d* tree algorithm on both high spatial and low spatial resolution split-window imager radiances is performed next. Specifically, the inputs to the *k-d* tree are the split-window 11 and 12 μm imager radiances at both the pixel and FOV spatial resolutions (from step 3); furthermore, the corresponding imager and sounder latitude and longitude values are used as additional predictors. The *k-d* tree input data has therefore *npix* (number of pixels in an imager granule) and 4 predictors (2 bands of radiances, as well as latitudes and longitudes). The outcome of the *k-d* tree search is a matrix of dimension *npix* x *N* containing the indices of the *N* sounder FOVs that are near the chosen pixel and best match the measured imager IR radiances.
5. For each FOV, the sounder spectral radiances are convolved with one or more spectral response functions for the imager band to be constructed. Thus, high-spectral resolution sounder radiances are reduced to narrowband imager-like radiances.
6. For each imager pixel, the mean is calculated of the convolved radiances for the *N* FOVs
7. Results are saved to mat files, which are Matlab 'save' files of binary data.
8. The binary results in the mat files are subsequently read in and appended to the VIIRS Level-1B NetCDF file. This is a Python routine that also computes scaled brightness temperatures, as is done with the measured VIIRS data.

We note that the inputs to the *k-d* tree are the split-window 11 and 12 μm imager radiances at both the pixel and FOV spatial resolution; for the latter the imager radiances are averaged that are geographically collocated to each sounder FOV. The corresponding imager and sounder latitude and longitude values are used as additional predictors. The *k-d* tree input data has therefore *npix* (number of pixels in an imager granule) and 4 predictors (2 radiance bands as well as latitudes and longitudes). The *k-d* tree search is solely based on imager radiances at the pixel resolution and averaged over the FOV resolution, and not on sounder radiance information. To be clear, only the split-window bands, i.e. MODIS bands 31 and 32 and VIIRS bands M15 and M16, are used in the *k-d* tree application to a granule.

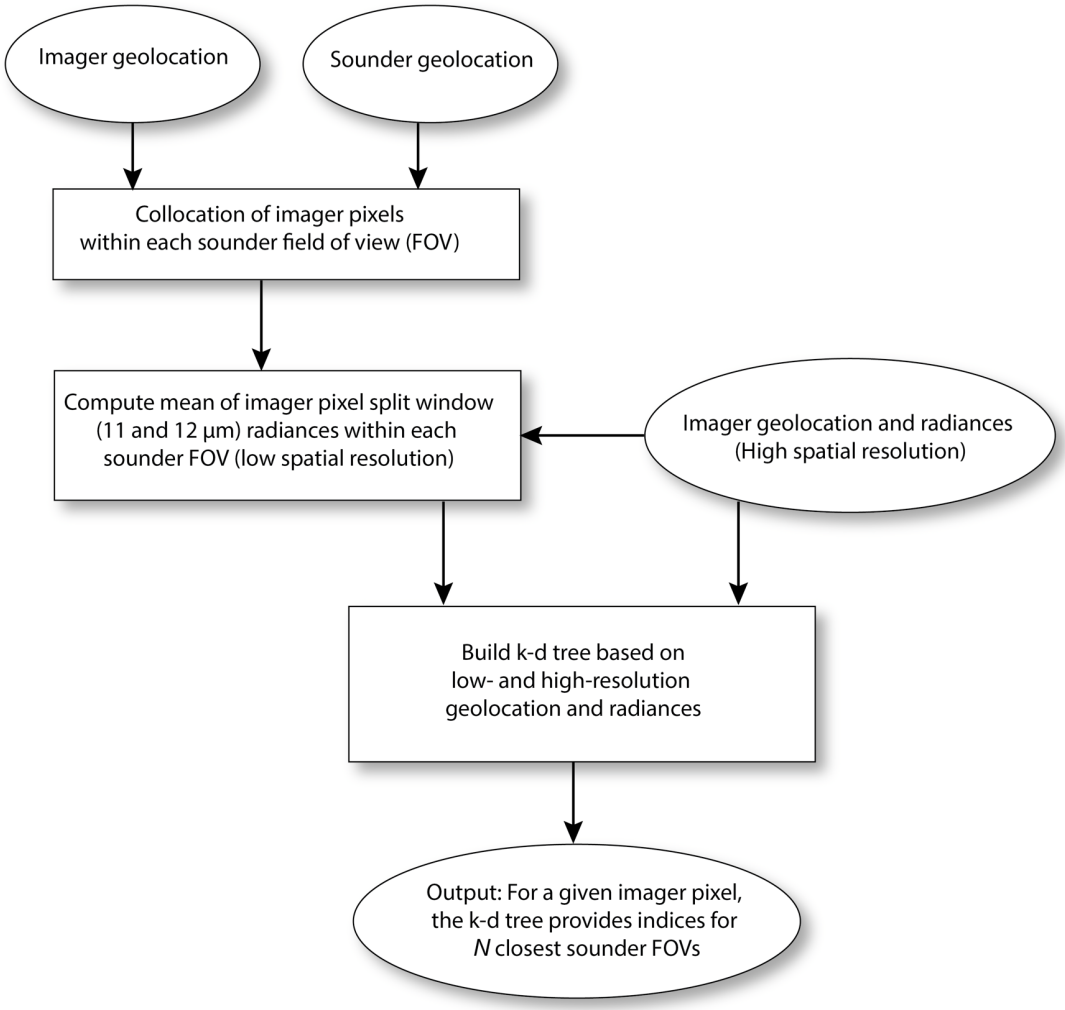

Figure 2: The process for creating a multidimensional search tree (*k-d* tree) using high spatial resolution (imager) radiance and geolocation information and low spatial resolution (sounder) geolocation information. Note that in this step, imager and sounder geolocation data are used but only imager radiances are used at both low and high spatial resolutions. No sounder radiance data are used in this step.

In the second step (Fig. 3), sounder spectral radiances for each FOV are convolved with the spectral response function (SRF) for the band to be constructed at imager pixel resolution. Thus, high-spectral resolution sounder radiances are convolved with a response function to match narrowband (i.e., imager-like) radiances while retaining the sounder's spatial resolution. The average of the convolved radiances for the *N* FOVs is associated with each imager pixel. This process is repeated for every imager pixel in the granule.

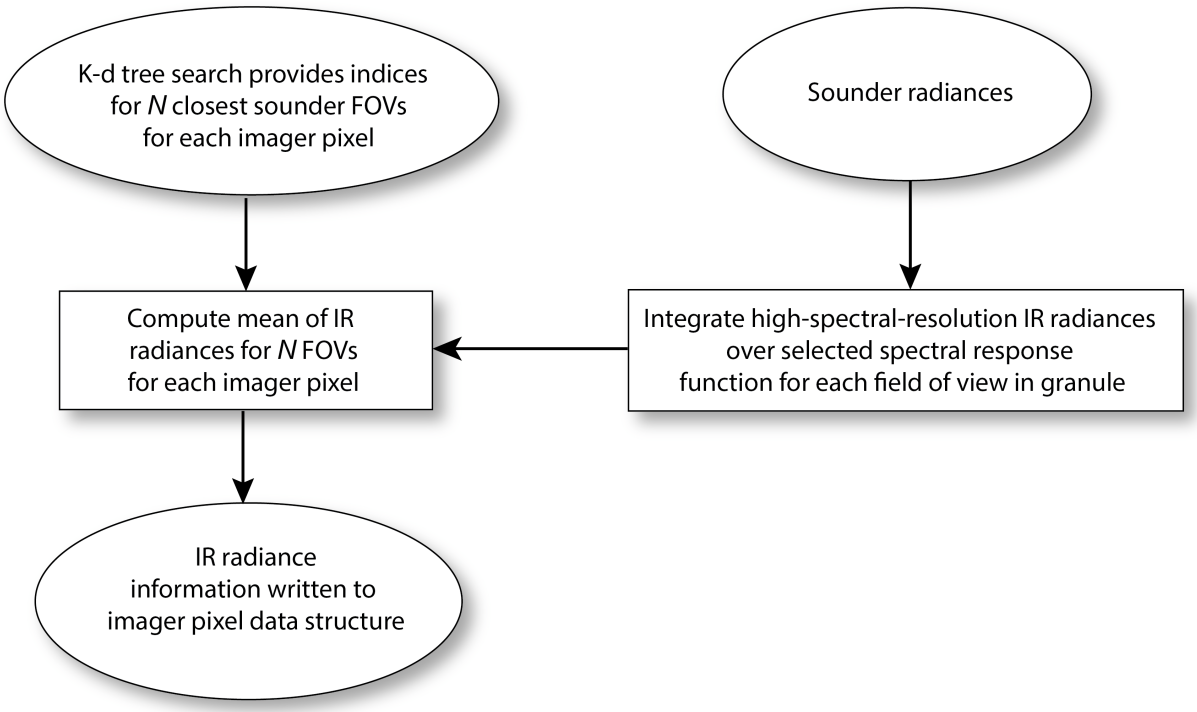

Figure 3: Each imager pixel uses the k-d tree to determine the 5 sounder fields-of-view that best match the IR window radiances and are located closely in geographic space. The convolved (integrated) radiances calculated for each of the sounder FOVs are averaged and then linked to the imager pixel as the "constructed" radiance.

2.4 Post-processing: appending IR band radiances into VIIRS Level-1B granule

Post-processing for the fusion band radiances includes conversion of the output to conform to instrument output format and convention. This permits the fusion data to be used in science software with minimal additional software modifications. The conversion is implemented as Python scripts, reading Matlab MAT files generated by the fusion science software and writing HDF4 or NetCDF4 output files depending on instrument convention.

The NASA VIIRS convention is NetCDF4 compliant to Climate and Forecasting (CF) metadata. Individual instrument channels are separate scaled-integer radiance variables in this format, with accompanying raw integer value look-up tables (LUT) providing corresponding brightness temperatures where relevant. As the fusion channels largely conform to MODIS spectral response functions, the brightness temperature LUTs are generated using established MODIS equations and coefficients. In the VIIRS Level-1B file, there is no set number of bands – each band is stored separately rather than stacked into a multidimensional array as in the MODIS Level-1B granules.

For MODIS-AIRS fusion, the format is HDF4 with channel stacking into a multidimensional array. We decided that providing drop-in replacement product files with channel substitution of fusion channels over native channels would be the simplest interface for down-stream science use. For the MODIS Level-1B files, the number of bands and relevant band information (e.g., central wavelengths; reflective versus IR thermal emission band, etc.) is set in each granule. To

change the number of bands would require users to change their software, a step that we wanted to avoid. Our goal was to work towards minimal impact for users.

2.5 Example of fusion process with a MODIS granule

An example is shown in Figure 4 for the case of a 5-minute granule on April 17, 2015 at 1435 UTC over the eastern Atlantic Ocean. In this scene (Fig. 4a), high clouds are white, low clouds are dark grey, and ocean is dark, i.e., cold targets are white and warm targets are dark. The range of radiances is from 2 to 6 W m^{-2} str^{-1} μm^{-1}. The 13.3-µm radiances shown in Fig. 4b are constructed from MODIS and AIRS data based on the logic in Figs. 2 and 3. For the results shown in this and following sections, *N* is set to 5, i.e., 5 AIRS FOVs are chosen for the radiance construction for each MODIS imager pixel. Note that the (measured – constructed) radiance differences in Fig. 4c are generally less than ±0.05 W m^{-2} str^{-1} μm^{-1} within the AIRS swath. Outside of the AIRS swath (denoted by the red lines in Fig. 4d), there tends to be a negative bias except when there is a cloud. The primary reason for the bias when there is no high cloud present is that we are not accounting for limb darkening outside of the AIRS swath, i.e., the absorption is increasing with path length. This could be corrected with use of a radiative transfer model but this has not yet been implemented. Fig. 4d shows the average distance between the 5 AIRS FOVs selected for each MODIS pixel. Within the sounder swath, the distances are generally less than 200km, while higher outside the swath as expected.

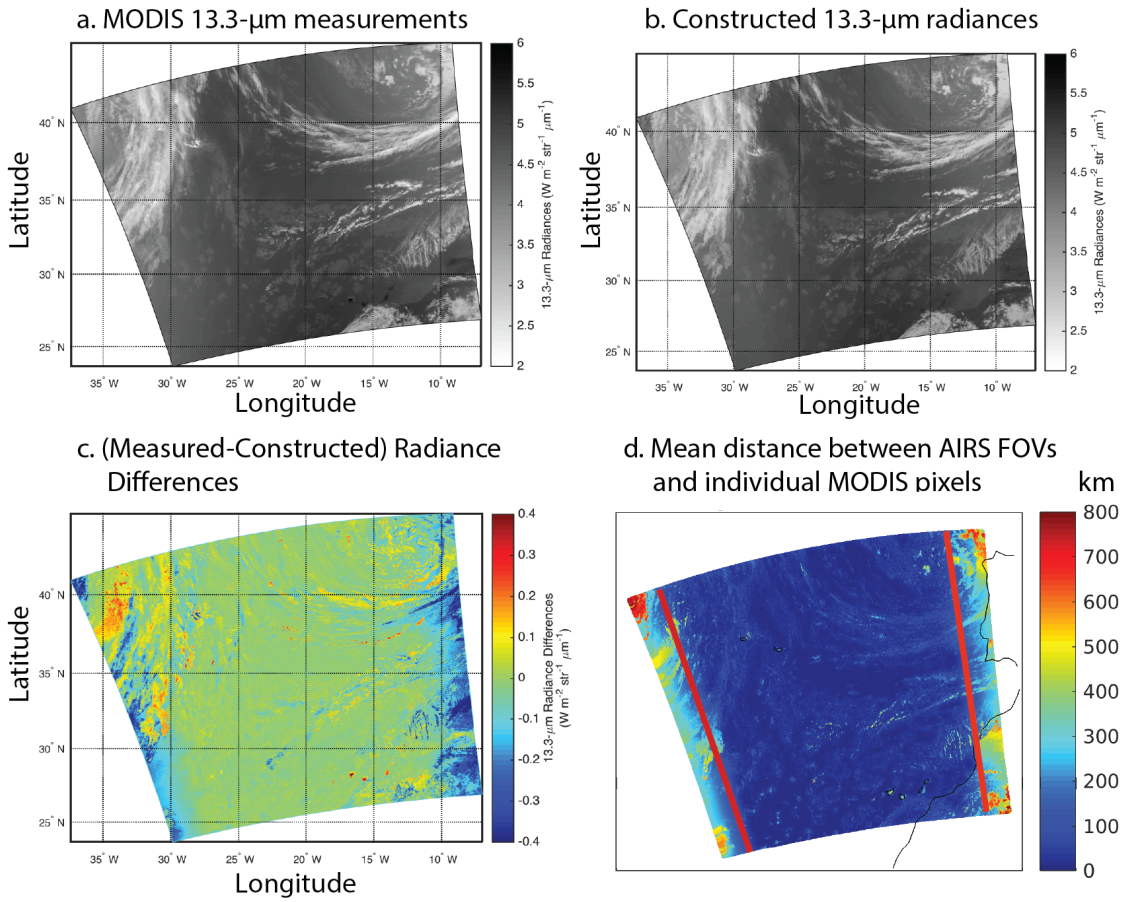

Figure 4: (a) Measured MODIS Band 33 (13.3-µm) radiances from a 5-minute granule on April 17, 2015 at 1435 UTC over the eastern Atlantic Ocean. High clouds are white, low clouds are dark grey, and ocean is dark. (b) Constructed MODIS 13.3-µm radiances, (c) pixel-level (measured – constructed) 13.3-µm radiance differences, and (d) mean distances between the 5 AIRS FOVs and the MODIS pixels. Note that within the AIRS swath (red lines), the mean distances are generally less than 200 km, while outside the AIRS swath, the distances increase as expected.

2.6 Assessment of radiance uncertainty

The means and root mean square errors (in radiance and brightness temperature units) of the 'observed minus fusion' differences are given in Table 3 for three other spectral bands for the full granule shown in Fig. 4 as well as the narrower region within the sounder swath. The MODIS bands in Table 3 are band 25 (4.52 µm) in the shortwave (SW) CO_2 spectral region, band 27 (6.72 µm) in the longwave (LW) H_2O region, and band 35 (13.9 µm) in the longwave CO_2 region. The differences are largest at the edge of the granule, where fewer sounder FOVs are available in close vicinity to a given imager pixel.

Table 3: Mean and RMS of 'observed minus fusion' radiance (and brightness temperature) differences for the full MODIS granule (1435 UTC, 17 April 2017) shown in Fig. 3. Values for the region within the sounder swath are in parentheses. From Weisz et al. (2017).

	Band 25 SW CO_2		Band 27 LW H_2O		Band 35 LW CO_2	
	Mean	RMS	Mean	RMS	Mean	RMS
Radiance [W m^{-2} sr^{-1} µm]	-0.003 (0.012)	0.012 (0.008)	-0.003 (-0.002)	0.063 (0.051)	-0.007 (-0.001)	0.045 (0.031)
Brightness Temperature [K]	-0.24 (0.07)	0.97 (0.60)	-0.07 (-0.06)	1.48 (1.15)	-0.13 (-0.01)	0.83 (0.57)

2.7 Data fusion application to VIIRS and CrIS radiances

The next step in the process is to apply the fusion approach to VIIRS and CrIS. Figure 5a shows the MODIS granule recorded on April 17, 2015 at 1435 UTC and the constructed 13.3-µm image based on VIIRS and CrIS at 1440 UTC is shown in Fig. 5b. The MODIS and VIIRS sensor overpasses are within 5 minutes of each other for this scene. The similarity of the detailed radiances between the two scenes is remarkable. Note that the constructed 13.3-µm channel covers the complete swath of the 750 m VIIRS measurements. Because the CrIS swath is narrower than the VIIRS swath, the constructed radiances are expected to be somewhat unreliable in the part of the VIIRS swath that lies outside the CrIS data. In the comparison with MODIS, there tends to be a warm bias in the constructed radiances for the non-cloudy pixels outside of the AIRS swath, i.e., the constructed MODIS radiances are higher than the measurements. However, there are cloudy pixels where the opposite is true, i.e., the constructed MODIS radiances are lower than those measured.

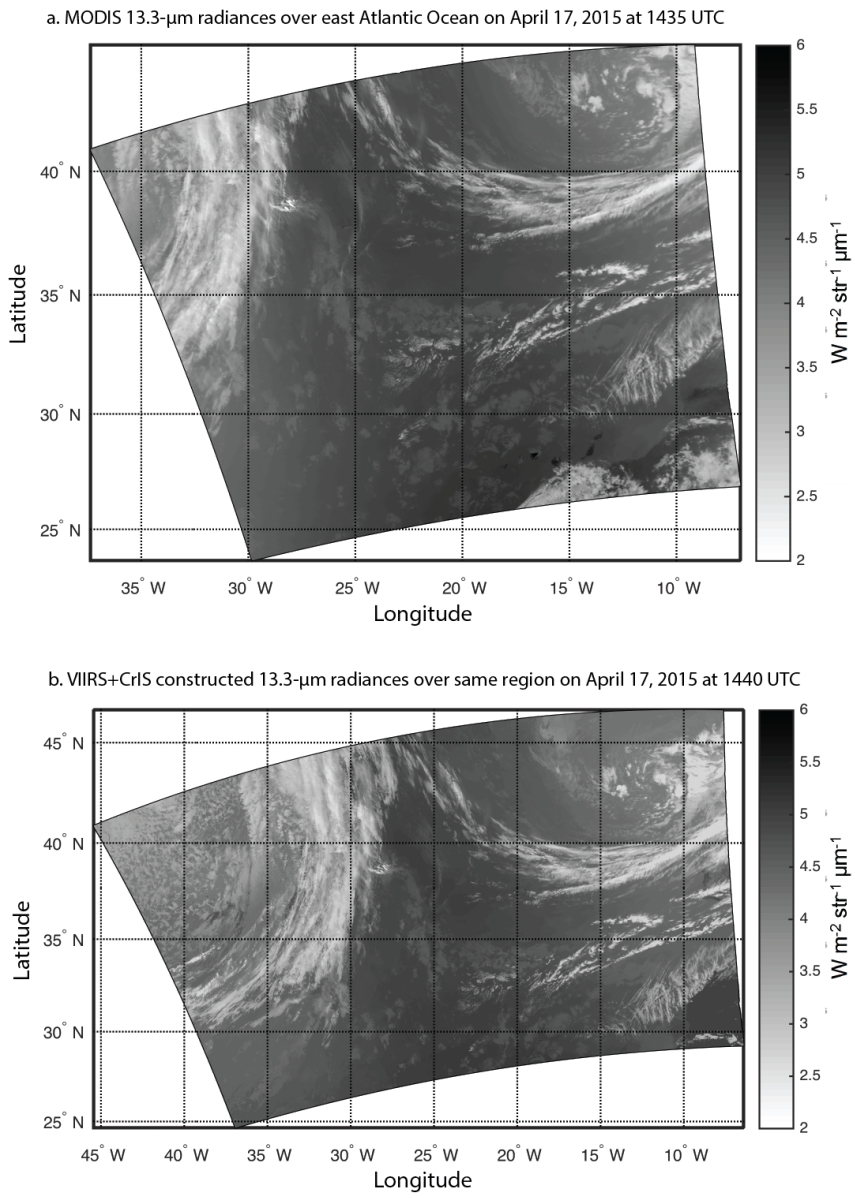

Figure 5: a. Measured MODIS Band 33 (13.3-µm) radiances from a 5-minute granule on April 17, 2015 at 1435 UTC over the eastern Atlantic Ocean. High clouds are white, low clouds are dark grey, and ocean is dark. (b) A scene constructed from VIIRS+CrIS data from an overpass about 5 minutes later than the Aqua overpass.

Since AIRS and CrIS have different scanning patterns, it is illustrative to show the CrIS scanning pattern superimposed on the VIIRS swath (see Fig. 6a). Note that in the center of the swath, the CrIS FOVs form a 3x3 array. As the CrIS scans, the FOVs begin to elongate and tilt, so the scanning pattern becomes quite complex. Away from the center of the swath, the FOVs begin to overlap each other, and there are some gaps that become evident. For comparison, the constructed 13.3-µm channel is shown in Fig. 6b. The broad cloud features are evident in Fig. 6a from the CrIS data alone, but the detail provided in the constructed band is missing.

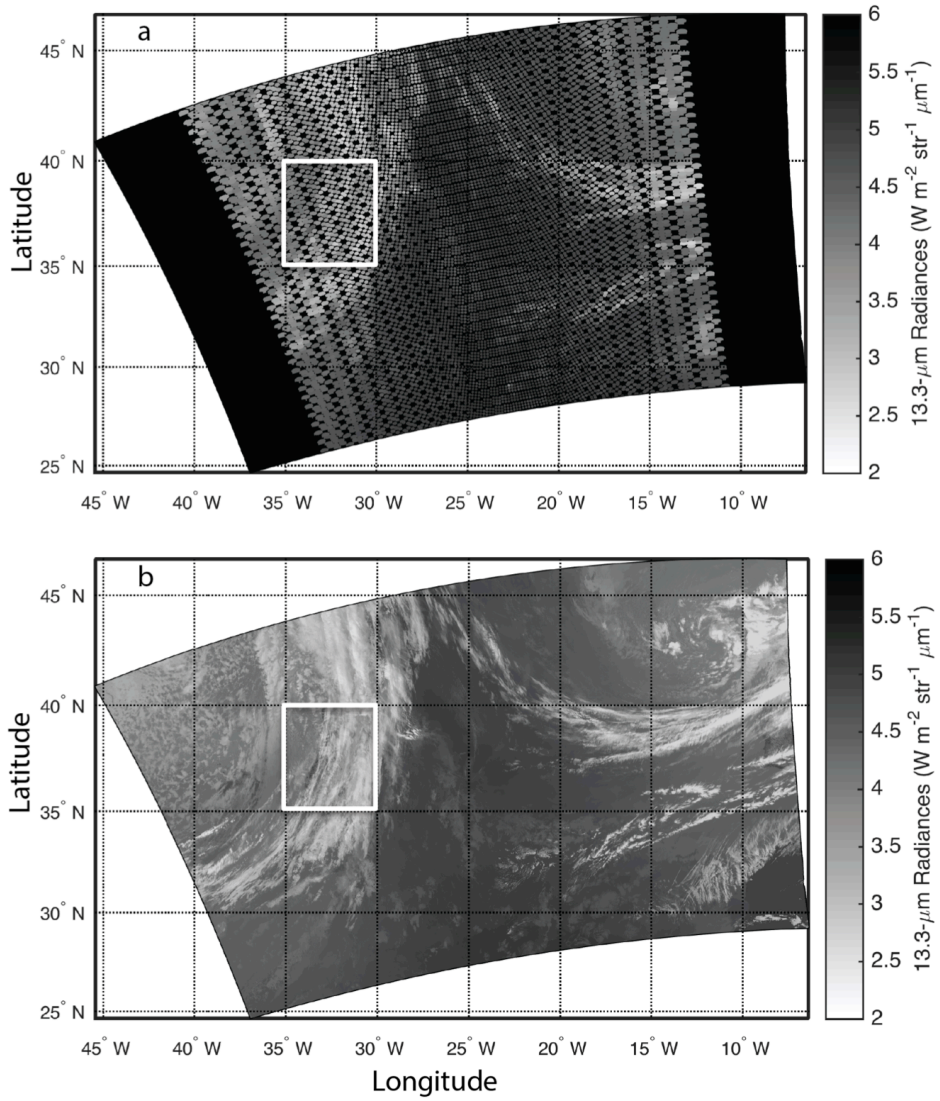

Figure 6: a. Measured CrIS 13.3-µm radiances superimposed over the VIIRS swath from a 5-minute granule on April 17, 2015 at 1440 UTC over the eastern Atlantic Ocean. The CrIS fields-of-view (FOVs) do not overlap near nadir but at higher viewing angles, the scan pattern becomes more complex and includes data gaps. (b) The 13.3-µm image constructed from VIIRS and CrIS data.

To illustrate the complexity of the CrIS scan pattern further away from nadir, Fig. 7 shows a 5˚ region as denoted by the white rectangle in Fig. 6a and 6b. Fig. 7a shows the CrIS FOVs for this region. For the purpose of this comparison, a single 13.3-µm radiance is derived for each FOV by integrating the CrIS radiances over the MODIS 13.3-µm spectral response function. Fig. 7b shows the constructed 13.3-µm radiances at the VIIRS spatial resolution of 750m.

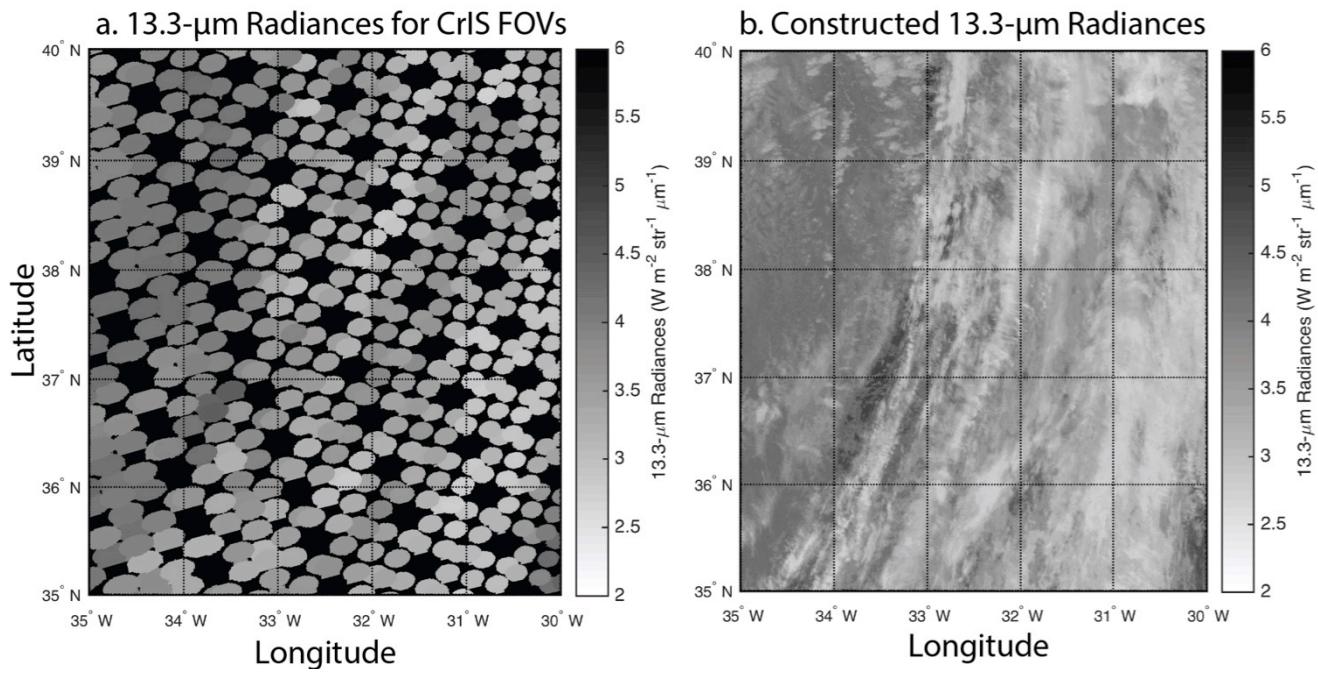

Figure 7: a. Measured CrIS 13.3-µm radiances for the subsetted region highlighted in Fig. 6a. The CrIS scan pattern becomes more complex away from nadir. There may be overlap between different FOVs. Also note the presence of data gaps. (b) The high spatial resolution 13.3-µm image constructed from VIIRS and CrIS data for the same highlighted region.

3. Global results from data fusion

3.1 MODIS radiance tests – limitation of sensor zenith angle

In this section, we further investigate the cold bias evident in the constructed radiances that are outside of the sounder (AIRS) swath. A full day of MODIS radiances are constructed and the nighttime 'real-constructed' radiance differences are shown in Figure 8. While not shown, the daytime results are similar. The imagery based on the measured 13.3-µm radiances is shown in Fig. 8a and the (real-constructed) 13.3-µm radiance differences are shown in Fig. 8b. As with the single granule shown in Fig. 4, there is a negative radiance bias outside of the AIRS swath where the fusion algorithm is basically extrapolating results, and the chosen FOVs for each pixel outside of the imager swath may not be very closely matched in radiances or situated closely to the pixel. If the imager sensor zenith angle is limited to ±57˚ as shown in Fig. 8c, most of the negative bias is removed from the scene. Where AIRS and MODIS overlap, the radiance differences are generally very small, with a slight increase related to cloud structure as shown in Fig. 4. We note in particular that there is no apparent issue in moving from land to ocean regardless of the land type, nor in moving from snow/ice to water at high latitudes. To summarize, the construction of a 13.3-µm channel seems to offer few artifacts, the radiance differences are small regardless of the surface, but increase slightly within a highly variable cloud field.

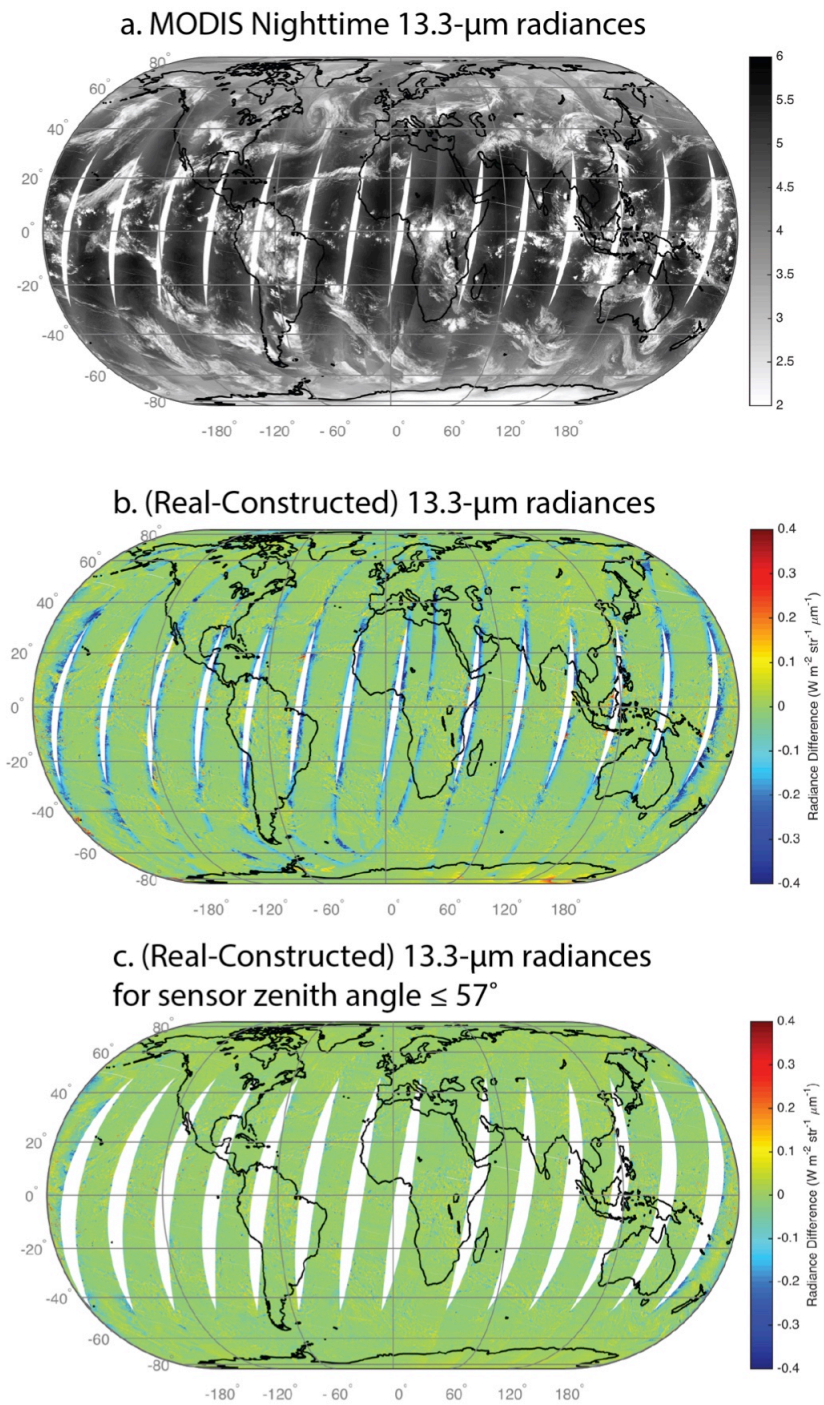

Figure 8: (a) Measured MODIS Band 33 (13.3-µm) nighttime radiances for April 17, 2015. High clouds are white, low clouds are dark grey, and ocean is dark. (b) (measured – constructed) 13.3-µm radiance differences for the full MODIS swath. Note that outside the AIRS swath, the constructed radiances tend to become colder leading to a negative radiance difference. (c) (measured – constructed) 13.3-µm radiance differences for the MODIS swath limited to sensor zenith angle ≤ 57˚.

A global example for MODIS and VIIRS daytime radiances corresponding to band 25 (4.52 µm) is shown in Fig. 9. The grayscale MODIS radiance measurements are shown in Fig. 9a. Figure 9b shows radiance differences (measured – fusion) based on MODIS for a swath limited to 57˚ in sensor zenith angle. The regions with more variability tend to occur over land and are associated with clear-sky conditions, but the differences are still generally low. This variability may be related to surface emissivity differences in the 11 and 12 µm bands, but this is still under investigation. The fusion process is applied to VIIRS+CrIS in Fig. 9c, again with the VIIRS swath limited to the extent of the CrIS swath at a sensor zenith angle of 60˚. Comparison of Fig. 9c to Fig. 9a show that the cloud features are very similar.

Figure 10 shows similar results as in Fig. 9, but for MODIS water vapor band 27 (6.72 µm). The MODIS (measured – fusion) radiance differences are higher than for band 25. The VIIRS fusion band image shown in Fig. 10c shows remarkable similarity to the measurements in Fig. 10a, at least in the "big picture". However, there are differences that become more apparent under scrutiny, such as the inability to capture features that have sharp gradients such as dry slots (higher latitudes). The use of sounder data tends to smooth out the sharp features that may be in the higher spatial resolution imager data. Additionally, water vapor can change rapidly with height in the troposphere, and this may also be an aspect that the fusion approach does not capture adequately.

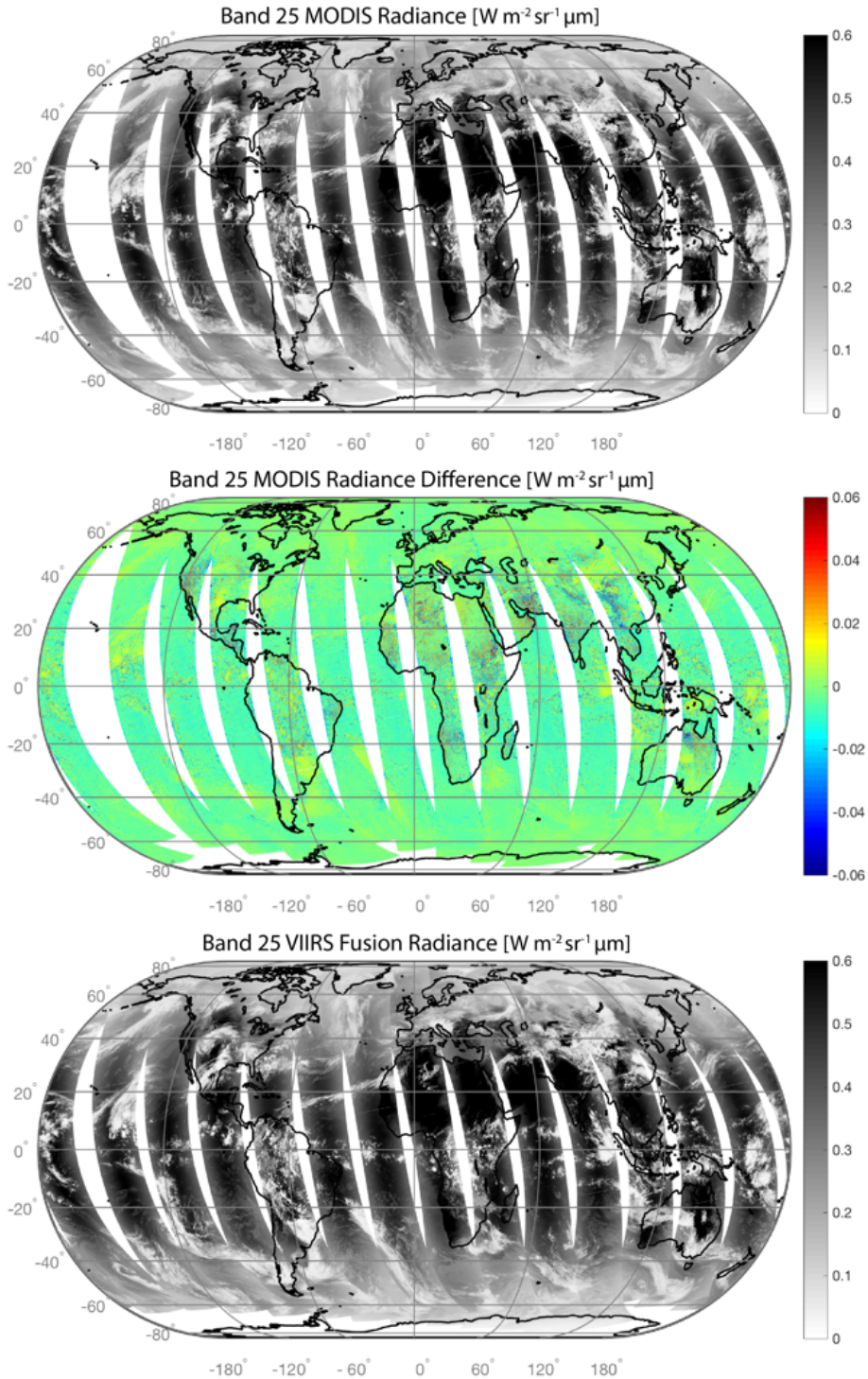

Figure 9: (a) Measured MODIS Band 25 (4.52-µm) daytime radiances for April 17, 2015 with the swath limited to sensor zenith angle ≤ 57˚. The swath is limited to mimic that portion of the data with complete AIRS coverage. High clouds are white, low clouds are dark grey, and warm surfaces are dark. (b) (measured – constructed) 4.52-µm radiance differences for the MODIS swath. Note that within the AIRS swath, the (measured – fusion) radiance differences are generally quite small. (c) Constructed 4.52-µm radiances for VIIRS based on CrIS data, for that portion of the VIIRS swath where there is complete CrIS coverage, i.e., sensor zenith angle ≤ 60˚. From Weisz et al. (2017).

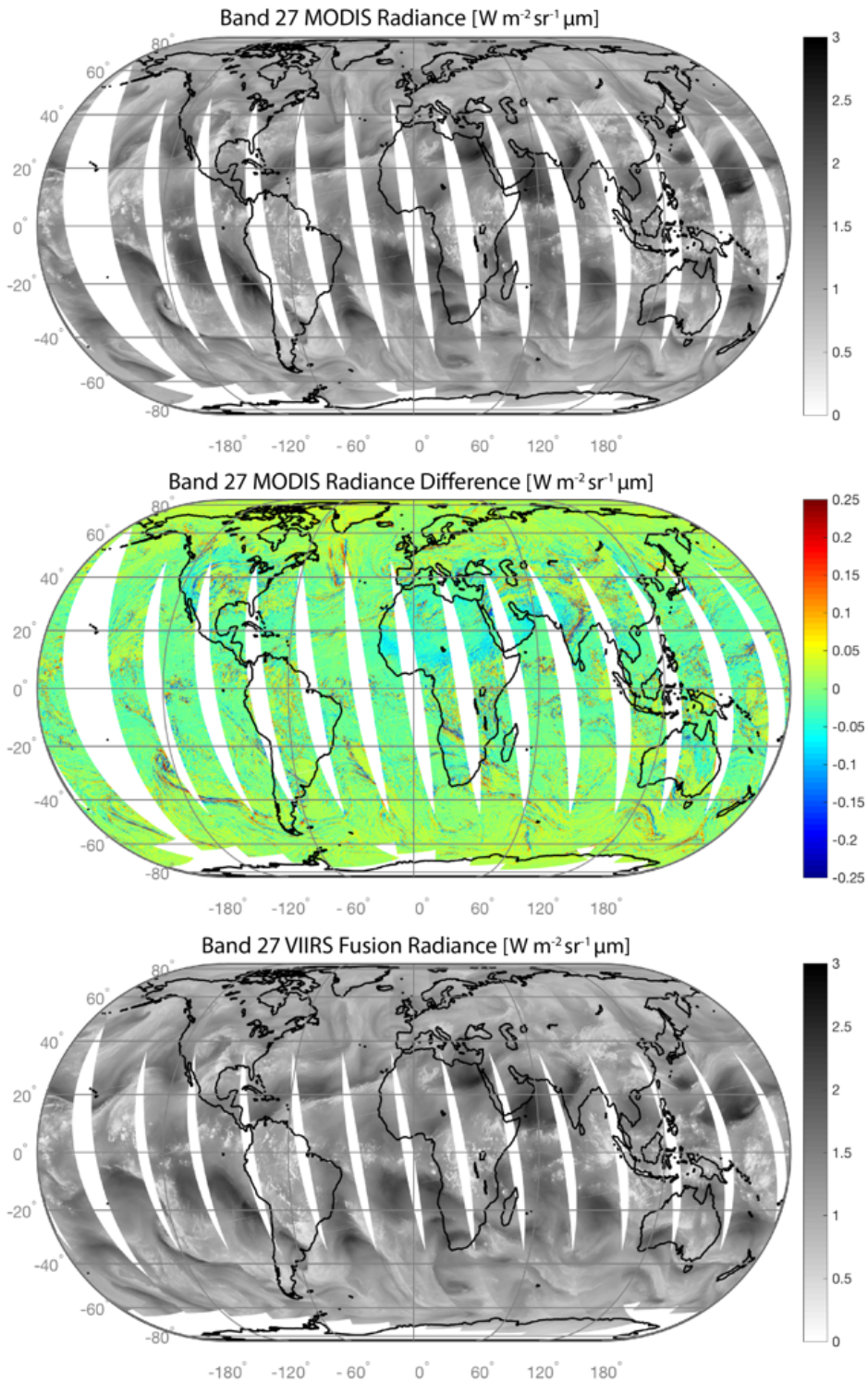

Figure 10: (a) Measured MODIS Band 27 (6.7-µm) daytime radiances for April 17, 2015. (b) MODIS Band 27 (measured – constructed) 6.7-µm radiance differences for the MODIS swath limited to sensor zenith angle ≤ 57˚. (c) Constructed 6.7-µm radiances for VIIRS based on CrIS data, for that portion of the VIIRS swath where there is complete CrIS coverage, i.e., sensor zenith angle ≤ 60˚. From Weisz et al. (2017).

4. Software and data management

The salient point to note is that mature software exists after undergoing a long development and testing process involving global MODIS+AIRS and VIIRS+CrIS data. Furthermore, software has also been developed to append these IR band radiances to an existing Level-1B file. For Aqua MODIS, the process replaces the original IR bands with the fusion-based bands in the MYD021KM files. This approach was chosen so that users could test our fusion-based granules without having to change any existing software or read routines. For VIIRS, the fusion-based bands are appended to the Level-1B NetCDF4 6-min granules. The VIIRS moderate resolution (750 m) granules contain 16 bands; the appended MODIS-like bands span bands 24 through 36 so that users of both MODIS and VIIRS Level-1B data will have continuity in how these band numbers are defined. Each imager-sounder pair has its own standalone software package to ease its use and maintenance in an operational setting. Each of our imager-sounder software packages consists of multiple modules that are all under version control.

Our software to construct IR radiances is a combination of Matlab and Python modules and has been implemented at the Atmosphere SIPS. The Matlab software performs the science involved with constructing, testing, and evaluating the fusion radiances. The Python modules perform imager-sounder geolocation, definition and application of the spectral response functions to CrIS data, and appending the fusion radiances to the VIIRS Level-1B granules in the VIIRS Level-1B format (NetCDF4). Each software module is fully documented and under version control at all times. The Atmosphere SIPS can construct supplementary IR bands for VIIRS and append all, or a subset, of the radiance bands into the VIIRS Level-1B granules for users. Given how the VIIRS Level-1B granule is structured, inclusion of the IR band radiances does not impact any existing applications. This software currently constructs radiances using the Aqua MODIS response functions for MODIS bands 24, 25, 27, 28, 30, and 33-36.

In addition to the IR band radiances, which use scaling factors similar to those used for other MODIS and VIIRS radiances, scaled brightness temperatures are also provided for each band.

At this time, it is unclear whether an archive will be built of the VIIRS Level-1B files with all the IR radiance bands appended, or whether the IR band radiances will be constructed and appended upon request by individual science teams. All operational software will continue to be available upon request through the SIPS along with documentation such as the Algorithm Theoretical Basis Document (ATBD) and related journal articles.

6. References

Aumann, H. H., M.T. Chahine, C. Gautier, M.D. Goldberg, E. Kalnay, L.M. McMillin, H. Revercomb, P.W. Rosenkranz, W.L. Smith, D.H. Staelin, L.L. Strow, and J. Susskind, 2003: AIRS/AMSU/HSB on the Aqua mission: Design, science objectives, data products, and processing systems. *IEEE Trans. Geosci. Remote Sensing*, **41**, 253-264.

Baum, B. A., W. P. Menzel, R. A. Frey, D. Tobin, R. E. Holz, S. A. Ackerman, A. K. Heidinger, and P. Yang, 2012: MODIS cloud top property refinements for Collection 6. *J. Appl. Meteor. Clim*., 51, 1145-1163.

Bentley, J. L., 1975: Multidimensional binary search trees used for associative searching. *Commun. ACM* 18(9), 509–517, http://dx.doi.org/10.1145/361002.361007.

Cao, C. et al., 2013: Visible Infrared Imaging Radiometer Suite (VIIRS) Sensor Data Record (SDR) User's Guide. NOAA Technical Report NESDIS 142.

Cross, J. I. Gladkova, W. P. Menzel, A. Heidinger, and M. D. Grossberg, 2013: Statistical estimation of a 13.3 µm Visible Infrared Imaging Radiometer Suite band using multisensor data fusion. *J. Appl. Remote Sens.* 7 (1), 073473. doi: 10.1117/1.JRS.7.073473

Han, Y., et al., 2013: Suomi NPP CrIS measurements, sensor data record algorithm, calibration and validation activities, and record data quality, *J. Geophys. Res. Atmos*., 118, 12,734–12,748, doi:10.1002/2013JD020344.

Heidinger, A. K., M. J. Pavolonis, R. E. Holz, B. A. Baum, and S. Berthier, 2010: Using CALIPSO to explore the sensitivity to cirrus height in the infrared observations from NPOESS/VIIRS and GOES-R/ABI. *J. Geophys. Res.*, **115**, D00l15, doi:10.1029/2009JD012379.

Menzel, W. P., R. Frey, H. Zhang, D. Wylie, C. Moeller, R. Holz, B. Maddux, B. A. Baum, K. Strabala, and L. Gumley, 2008: MODIS global cloud-top pressure and amount estimation: algorithm description and results. *J. Appl. Meteor. Climatol.*, **47**, 1175-1198.

Salomonson, V. V., W. L. Barnes, P. W. Maymon, H. E. Montgomery, and H. Ostrow, 1989: MODIS: Advanced Facility Instrument for Studies of the Earth as a System, *IEEE Trans. Geosci. Remote Sens.*, **27**, 145-153.

Weisz, E., B. A. Baum, and W. P. Menzel, 2017: Fusion of satellite-based imager and sounder data to construct supplementary high spatial resolution narrowband IR radiances. *J. Appl. Remote Sens.* **11**(3), 036022 (2017), doi: 10.1117/1.JRS.11.036022.